Science Bulletin 70 (2025) 2088–2093

Contents lists available at ScienceDirect

Science Bulletin

journal homepage: www.elsevier.com/locate/scib

Science Bulletin
www.scibull.com

Article

Emergence of nodal-knot transitions by disorder

Ming Gong [a,1], Peng-Lu Zhao [b,1], Hai-Zhou Lu [c,d,*], Qian Niu [b,e,f], X. C. Xie [a,g,h]

[a] International Center for Quantum Materials, School of Physics, Peking University, Beijing 100871, China
[b] Department of Physics, University of Science and Technology of China, Hefei 230026, China
[c] State Key Laboratory of Quantum Functional Materials, Department of Physics, and Guangdong Basic Research Center of Excellence for Quantum Science, Southern University of Science and Technology (SUSTech), Shenzhen 518055, China
[d] Quantum Science Center of Guangdong-Hong Kong-Macao Greater Bay Area (Guangdong), Shenzhen 518045, China
[e] CAS Key Laboratory of Strongly-Coupled Quantum Matter Physics, University of Science and Technology of China, Hefei 230026, China
[f] International Center for Quantum Design of Functional Materials, University of Science and Technology of China, Hefei 230026, China
[g] Interdisciplinary Center for Theoretical Physics and Information Sciences, Fudan University, Shanghai 200433, China
[h] Hefei National Laboratory, Hefei 230088, China

ARTICLE INFO

Article history:
Received 16 January 2025
Received in revised form 4 March 2025
Accepted 15 April 2025
Available online 2 May 2025

Keywords:
Nodal-knot
Disorder
Topological phase transition
Renormalization group

ABSTRACT

Under certain symmetries, degenerate points in three-dimensional metals form one-dimensional nodal lines. These nodal lines sometimes exhibit intricate knotted structures and have been studied in various contexts. As one of the most common physical perturbations, disorder effects often trigger novel quantum phase transitions. For nodal-knot phases, whether disorder can drive knot transitions remains an open and intriguing question. Employing renormalization-group calculations, we demonstrate that nodal-knot transitions emerge in the presence of weak disorder. Specifically, both chemical-potential-type and magnetic-type disorders can induce knot transitions, resulting in the emergence of distinct knot topologies. The transition can be quantitatively characterized by changes in topological invariants such as the knot Wilson loop integrals. Our findings open up a new avenue for manipulating the topology of nodal-knot phases through disorder effects.

1. Introduction

In the 1860s, Lord Kelvin's vortex atom theory introduced the concept of knots to physics, which was further developed by Peter Tait [1,2]. Despite its unfortunate failure, the efforts made by Kelvin and Tait significantly advanced the mathematical study of knot theory [1,2]. A century later, the development of topological quantum field theory revitalized knot theory, paving the way for fault-tolerant quantum computation [3–7]. To this day, the development of knot theory has far exceeded expectations, and knot-like states may even play an important role in the formation of the early universe [8].

As the condensed matter counterpart of topological quantum field theories, topological bands serve as ideal platforms for studying the emergence of novel phenomena. Specifically, degenerate points of three-dimensional (3D) topological bands can form one-dimensional (1D) nodal lines under the protection of symmetries [9,10]. These nodal lines provide a rich landscape of knots (nodal-knots) [11–25], and have been studied across a wide range of physical systems[11,26–30], including ultra-cold atoms [31–36], photonics [37–42], acoustics [43–47], and topological circuits [48–50]. The focus has also been extended from Hermitian physics to non–Hermitian physics [46,51–58].

Regardless of the systems that realize nodal-knots, a fundamental question is how these knotted structures can be tuned through perturbations. Unlike traditional symmetry-protected topological phases [59–61], the flexibility in the ways that 1D nodal lines are embedded into the 3D Brillouin zone to form knots enables the manipulation of nodal-knot structures. On the other hand, it is well-known that disorder effects can significantly renormalize dispersions and even cause localization transitions [62,63]. Consequently, quantum phase transitions can be triggered, and novel orders may emerge. Therefore, a fundamental and intriguing question naturally arises: Can nodal-knot phases of matter be manipulated by disorder?

In this work, we address this question by asserting that knot transitions of nodal-knot phases can be triggered by different types of disorder. Employing two-band models of semimetallic systems

* Corresponding author.
E-mail address: luhz@sustech.edu.cn (H.-Z. Lu).
[1] These authors contributed equally to this work

https://doi.org/10.1016/j.scib.2025.04.061

that host nodal-knot degeneracies, we study the evolution of nodal-knots with various knot topologies under weak disorder. With the help of renormalization-group (RG) calculations, we find that both chemical-potential-type disorder and magnetic-type disorder can trigger transitions in knot structures. Different types of disorder lead to the evolution of nodal-knots into different knot structures, as sketched in Fig. 1.

Mathematically, these knot transitions can be characterized by the knot Wilson loop integrals, which are knot invariants, and their change can be detected through the de Haas-van Alphen experiment. Our results uncover the fascinating interplay between knots, topological phases, and disorder effects and provide valuable insights for the study of nodal-knots in disordered systems across diverse backgrounds.

2. Model for 3D nodal-knots

To begin with, we construct the Hamiltonian for 3D nodal-knots. A general two-band Hamiltonian reads $H(\boldsymbol{k})=f_0(\boldsymbol{k})\sigma_0+\sum_{i=x,y,z}f_i(\boldsymbol{k})\sigma_i$, where σ_i are the Pauli matrices. In the presence of chiral symmetry $\mathcal{S}=\sigma_z$, the Hamiltonian satisfies $\mathcal{S}H(\boldsymbol{k})\mathcal{S}^{-1}=-H(\boldsymbol{k})$, which forces the σ_0 and σ_z terms to vanish. Then

$$H(\boldsymbol{k})=f_x(\boldsymbol{k})\sigma_x+f_y(\boldsymbol{k})\sigma_y. \tag{1}$$

The models that host different types of nodal-knots can be obtained by setting [12,13]

$$f_x(\boldsymbol{k})=\mathrm{Re}\mathcal{F}_{pq}(\boldsymbol{k}),\ f_y(\boldsymbol{k})=\mathrm{Im}\mathcal{F}_{pq}(\boldsymbol{k}), \tag{2}$$

where

$$\mathcal{F}_{pq}(\boldsymbol{k})=v_p(k_x+\mathrm{i}k_y)^p+v_q[k_z+\mathrm{i}(\lambda_1-\lambda_2k^2)]^q+m_1+\mathrm{i}m_2. \tag{3}$$

Here, $k^2=\sum_{i=x,y,z}k_i^2$, p and q are integers. The parameters $v_p, v_q, \lambda_1, \lambda_2, m_1$, and m_2 govern the shape of the nodal-knot. The degenerate points with $E(\boldsymbol{k})=\sqrt{f_x^2(\boldsymbol{k})+f_y^2(\boldsymbol{k})}=0$ determine the nodal lines in momentum space. When $v_p=v_q\neq 0, m_1=m_2=0$, $\lambda_2=0.5$, and $\lambda_1>0$, the nodal line of $\mathcal{F}_{pq}(k)$ forms the torus knot (or link) of type (p,q), thus different choices of (p,q) in $H(\boldsymbol{k})$ yield different nodal-knots. For example, $(2,2)$-the Hopf link, $(2,3)$ and $(3,2)$-the trefoil knot, and $(3,3)$-the valknut. When p and q are relatively prime to each other, the nodal-knot is connected (such as the trefoil knot), otherwise, it is disconnected (such as the Hopf link). The nodal lines of $H(\boldsymbol{k})$ are oriented, similar to the superconducting or superfluid vortex lines [64]. The orientation is determined by the unit tangent vector $\boldsymbol{T}(\boldsymbol{k}_0)$ [18] at point $\boldsymbol{k}_0$.

3. Disorder and renormalization

We model the disorder potential by a coupling term $H_{\mathrm{dis}}=\int \mathrm{d}^3\boldsymbol{r}U_v(\boldsymbol{r})\psi^\dagger(\boldsymbol{r})\sigma_v\psi(\boldsymbol{r})$, where $v=0$ denotes the chemical-potential type disorder and σ_v with $v=x,y,z$ denote the magnetic-type disorders in three directions [65]. $U_v(\boldsymbol{r})$ is the disorder potential of Gaussian white noise with probability distribution $p[U_v(\boldsymbol{r})]\propto\exp[-1/2\Delta_vU_v^2(\boldsymbol{r})]$ and spatial correlation $\langle U_v(\boldsymbol{r})\rangle=0$, $\langle U_v(\boldsymbol{r})U_\rho(\boldsymbol{r}')\rangle=\delta_{v\rho}\delta(\boldsymbol{r}-\boldsymbol{r}')$. Through the replica method [62,63,66], the fermionic mode $\psi(\boldsymbol{r},\tau)$ is replicated into N copies as $\psi_i(\boldsymbol{r},\tau)\,(i=1,\cdots,N)$ (Supplementary material Sect. I). In this way, the ensemble average results in an effective attractive interaction between replica fields with disorder strength Δ_v. The total action (Supplementary material Sect. I) comprises a free and a disorder part. We note that although chiral symmetry is externally broken by σ_z disorder, it is restored after disorder averaging, since $\langle U_z(\boldsymbol{r})\rangle=0$.

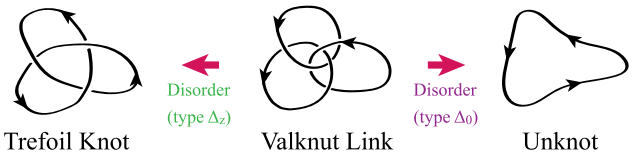

Fig. 1. Schematics of the knot transition of nodal-knots in the presence of disorder. The nodal line features a valknut linked structure (middle) in the clean limit. Under different types of disorders (highlighted with different colors), it can undergo transitions into a trefoil knot (left) or a single unknot (right).

To study how the band parameters $v_p, v_q, \lambda_1, \lambda_2, m_1$, and m_2 are renormalized by disorder strength $\Delta_{0,x,y,z}$, we then perform the Wilsonian momentum-shell RG calculations for the total action, with details shown in Supplementary material [63,67,68]. We set the momentum cut off as Λ. By integrating the fermionic modes inside the momentum-shell defined by $\mathrm{e}^{-\mathrm{d}l}\Lambda<|\boldsymbol{k}|<\Lambda$ and rescaling the momentum as $\boldsymbol{k}\to\mathrm{e}^{-\mathrm{d}l}\boldsymbol{k}$, we investigate the running of band parameters and disorder strengths $\Delta_{0,x,y,z}$ with respect to the running scale l. We consider one type of disorder at a time, taking the chemical-potential-type disorder Δ_0 and the magnetic-type disorder Δ_z as examples. Parameters $v_p, v_q, \lambda_1, \lambda_2$ are not renormalized by disorder and only do scale transformations. The RG equations for m_1, and m_2 read

$$\begin{aligned}\mathrm{d}m_1/\mathrm{d}l&=m_1+(-\Delta_0+\Delta_z)\mathcal{G}_1^x,\\ \mathrm{d}m_2/\mathrm{d}l&=m_2+(-\Delta_0+\Delta_z)\mathcal{G}_1^y,\end{aligned} \tag{4}$$

and the RG equations for Δ_0 and for Δ_z are

$$\begin{aligned}\mathrm{d}\Delta_0/\mathrm{d}l&=-\Delta_0+2\Delta_0^2(\mathcal{G}_2^{xx}+\mathcal{G}_2^{yy}),\\ \mathrm{d}\Delta_z/\mathrm{d}l&=-\Delta_z-2\Delta_z^2(\mathcal{G}_2^{xx}+\mathcal{G}_2^{yy}).\end{aligned} \tag{5}$$

The details for $\mathcal{G}_1^{(x/y)}$ and $\mathcal{G}_2^{(xx/yy)}$ can be found in Supplementary material.

The band parameters $v_p, v_q, \lambda_1, \lambda_2, m_1$, and m_2 renormalized by disorder deviate from their bare values, potentially resulting in distinct knot structures. In other words, disorder may trigger the emergence of knot transitions. We analyse the renormalization of the parameters by numerically solving the RG equations. As an example, we take $p=q=2$, and set the initial conditions at $l=0$ as $v_p(0)=v_q(0)=0.1, m_1(0)=m_2(0)=0, \lambda_1(0)=0.4$, and $\lambda_2(0)=0.5$. This set of parameters describes the hopf-linked nodal-knot in the clean limit (corresponding to the nodal-knot configuration in the absence of the disorder effect). The momentum cut off takes $\Lambda=5$. We show the results of the RG flow of m_1 in Fig. 2a and b under different initial disorder strength $\Delta_0(l=0)$ or $\Delta_z(l=0)$, together with the RG flows of Δ_0 and Δ_z in Fig. 2d and e. Here, m_2 keeps zero for the momentum-shell integration forces $\mathcal{G}_1^y$ to vanish. Clearly, both Δ_0 and Δ_z can drive the emergence of m_1, but in opposite signs. Similar results also hold for $p=q=3$, the valknut link (Fig. 3a and b). This strongly implies that different types of disorders can trigger different knot transitions. However, only the RG flow of these parameters is not adequate for displaying the features and types of the knot transitions; a more intuitive mathematical object, e.g., a topological invariant, is needed.

4. Knot invariants and knot transitions in (2,2) and (3,3) systems

Unlike band topological numbers such as TKNN numbers [69] and Z_2 numbers [59–61] that unambiguously characterize the symmetry-protected topological phases, the complexity of knots

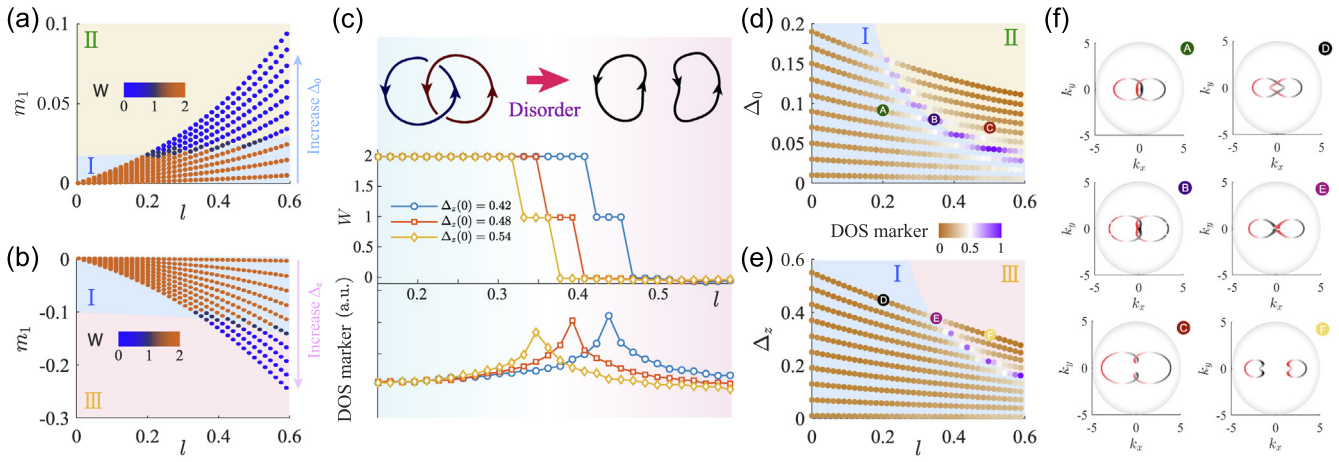

Fig. 2. RG flows of Hopf linked nodal-knots. (a), (b) The RG flows of m_1 under the renormalization of Δ_0 and Δ_z, respectively. The flow curves are colored by the knot Wilson loop W, and colored regions denote I the Hopf link, II the unknot, and III the unlink. (c) The RG flows of the knot Wilson loop (upper panel) and the DOS marker (lower panel) under the renormalization of Δ_z with different initial values. (d), (e) The RG flows of Δ_0 and Δ_z, respectively. The flow curves are colored by the DOS marker. The colored regions I, II, and III are the same as those in (a) and (b). The corresponding nodal-knot configurations of representative points labeled A–F on the RG curves are plotted in (f), colored by the y-component of unit tangent vector $T_y(\boldsymbol{k})$.

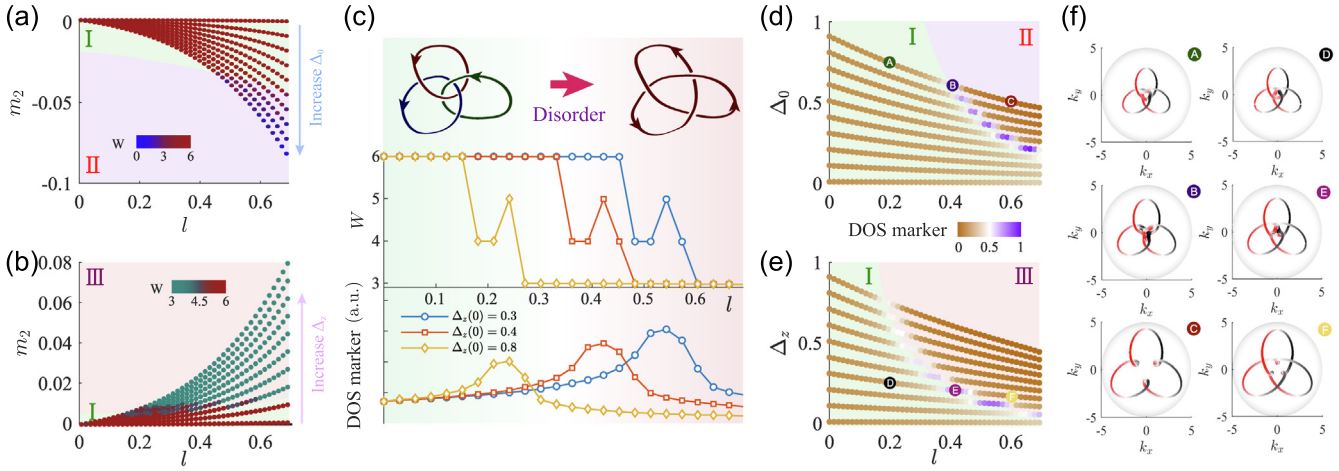

Fig. 3. RG flows of valknut linked nodal-knots. (a), (b) The RG flows of m_2 under the renormalization of Δ_0 and Δ_z, respectively. The flow curves are colored by the knot Wilson loop W, and colored regions denote I the valknut link, II the unknot, and III the trefoil knot. (c) The RG flows of the knot Wilson loop (upper panel) and the DOS marker (lower panel) under the renormalization of Δ_z with different initial values. (d), (e) The RG flows of Δ_0 and Δ_z, respectively. The flow curves are colored by the DOS marker. The colored regions I, II, and III are the same as those in (a) and (b). The corresponding nodal-knot configurations of representative points labeled A-F on the RG curves are plotted in (f), colored by the y-component of unit tangent vector $T_y(\boldsymbol{k})$.

makes it mathematically impossible to find a knot invariant that can provide a one-to-one characterization of the knot configuration. Nevertheless, knot invariants, the jumps of which can adequately reveal nodal-knot transitions, can still be calculated. Here, we adopt the knot Wilson loop integral W to determine the nodal-knot transitions [5,15]. The knot Wilson loop integral is

$$W(L_1,\cdots,L_N)=\frac{1}{\pi}\oint_{\boldsymbol{l}\in L_1,\cdots,L_N}\boldsymbol{A}(\boldsymbol{k})\cdot \mathrm{d}\boldsymbol{l}. \tag{6}$$

Here, $L_1,\cdots,L_N$ denotes the nodal loops oriented by N, and the orientation of the integral path $\boldsymbol{l}$ is determined by the tangent vector $\boldsymbol{T}(\boldsymbol{k}_0)$. $\boldsymbol{A}(\boldsymbol{k})=-\mathrm{i}\langle u_{\boldsymbol{k}}|\partial_{\boldsymbol{k}}|u_{\boldsymbol{k}}\rangle$ is the Berry connection. Mathematically, $W(L_1,\ldots,L_N)$ is the sum of the linking numbers Ψ_{ij} of loops L_i and L_j if $i\neq j$, and Ψ_{ii} would be the Gauss linking number of the loop L_i and its frame [1,2]. To faithfully reflect the knot topology, a proper frame should be chosen such that an unknotted loop has no contribution to W. Physically, the knot Wilson loop integral W reflects the Berry phase accumulated by electrons as they move along the intertwined nodal lines. For the Hopf-linked nodal-knot, each of the electrons moving along the nodal loops L_1 and L_2 gains π Berry phase, thus W = 2. For the valknut link, each nodal loop interlocks with the other two, and each gains 2π Berry phase, leading to W = 6 in total. With this mathematical tool in hand, we can view the nodal-knot transitions more intuitively. We color the RG flows in Fig. 2a and b with the calculated knot Wilson loop integral W. Moreover, to demonstrate the phase boundaries of nodal-knot transitions more comprehensively, we have supplemented the calculation with the density of states (DOS) marker colored in the RG flow curves of Δ_0 and Δ_z in Fig. 2d and e, which counts the number of states within the energy window $[0,\epsilon]$ with ϵ an extremely small energy scale. It is worth noting that this DOS marker is different from the real DOS like that was studied in Weyl semimetals [70–72]. There, the disorder can broaden the DOS and lead to Fermi surface instabilities, thus falling into the Landau paradigm and different from our study on the Lifshitz transition of the nodal-knots.

At the transition points, the nodal lines should touch and then separate and reconnect, leading to the divergence of the DOS markers. In this way, the transition boundaries can be determined jointly by W and the DOS markers. Specifically, we take three curves in Fig. 2b and plot them in terms of W and the DOS marker in Fig. 2c. It is clear that the knot Wilson loop integral W drops from 2 to 0, and for each curve, the DOS markers show clear peaks at the transition points.

To visualize the renormalized nodal-knot configurations, we select six points on the RG flow curves marked A–F in Fig. 2d and e. The corresponding knot configurations are displayed in Fig. 2f. Interestingly, although both Δ_0 and Δ_z drive the transition of W from 2 to 0, the results of these transitions are different. As shown in Fig. 2f, Δ_0 drives the transition from a Hopf link (A or D) to an unknot (C), while Δ_z drives the transition to an unlink (F). This difference stems from their renormalization effect on the parameters m_1 and m_2 with opposite signs. Therefore, we can divide the RG flow diagrams into regions I (Hopf link), II (unknot), and III (unlink) (shown in Fig. 2a, b and d, e).

Similar to the Hopf link, the valknut nodal-knot with $p=q=3$ also experiences different transitions under different types of disorder. In parallel to the Hopf link, we show the results of RG flow and the corresponding W and DOS markers (Fig. 3a–e). Different from the Hopf link, only m_2 survives. We see that under the renormalization of Δ_0, W jumps from 6 to 0, while under Δ_z, W jumps from 6 to 3, which is distinct from the Hopf links. Moreover, representative nodal-knot configurations shown in Fig. 3f suggest that we can similarly divide the RG flow into regions I, II, and III, which describe the nodal-knot configurations of valknut, unknot, and trefoil knot, respectively. Note that under Δ_z, the originally linked valknut evolves into the trefoil knot, which is a knotted structure, in sharp contrast to the case of the Hopf link which evolves into either unknot or unlink.

As summarized in Fig. 4 and Table 1, we can conclude that the ability of different types of disorder to induce different types of nodal-knot transitions is universal. Especially, the presence of magnetic disorders can diversify the knot configurations (see Table 1), giving rise to the emergent of non-trivial nodal-knots from their clean limit. This finding plays a crucial role in realizing and manipulating topological knotted phases in various systems in the future.

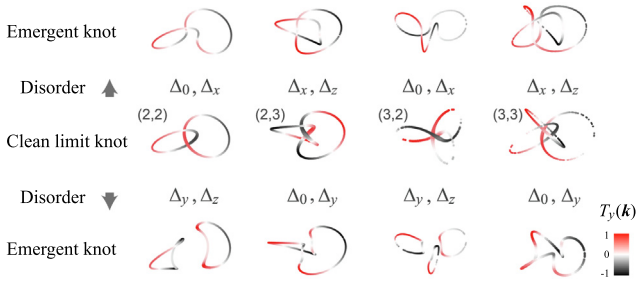

Fig. 4. Summary of the emergent knot configurations under different types of disorders. The middle line of the figure shows the clean limit nodal-knots, with various (p,q). Specifically, $(2,2)$-the Hopf link, $(2,3)$ and $(3,2)$-the trefoil knot, and $(3,3)$-the valknut. The y-component of unit tangent vector $T_y(\boldsymbol{k})$ is colored on the nodal-knots.

5. Phase shifts in quantum oscillation experiments

Experimentally, determining the transition of the Fermi surface topologies (i.e., Lifshitz transition) is typically accomplished by combining transport measurements with quantum oscillation experiments. Therefore, we propose a potentially feasible way to reflect the nodal-knot structures and their transitions through de Haas-van Alphen oscillation or Shubnikov-de Haas oscillation experiment [73–76], as demonstrated in Fig. 5. Taking the Hopf link as an example, before the transition occurs, a magnetic field is applied perpendicular to one of the nodal loops, which is the 1D Fermi surface of the system at $\mu = 0$. According to the semiclassical equations of motion [77]

$$\begin{aligned} \dot{\boldsymbol{r}} &= \partial\epsilon(\boldsymbol{k})/\hbar\partial\boldsymbol{k} - \dot{\boldsymbol{k}} \times \boldsymbol{\Omega}(\boldsymbol{k}), \\ \dot{\boldsymbol{k}} &= -e/\hbar\boldsymbol{E} - e/\hbar\dot{\boldsymbol{r}} \times \boldsymbol{B}, \end{aligned} \tag{7}$$

electrons undergo cyclotron motion in momentum space, moving perpendicular to the magnetic field and around the nodal loop, as indicated by the loops of different colors in the left panel of Fig. 5. The area enclosed by its cyclotron orbit in momentum space is denoted by A_{orb}. When the magnetic field changes, the DOS exhibits periodic oscillations with a period A_{orb}/B, as shown in the right panel of Fig. 5. Under the renormalization of disorder, the linked structure evolves to be unlinked, as shown in the middle panel of Fig. 5. Applying a magnetic field in this situation still results in quantum oscillations, but the phase of the oscillation with A_{orb}/B may shift. When two nodal loops are linked together, the cyclotron motion orbit of electrons on one nodal loop will encircle the other nodal loop. According to the Landau quantization rule

$$A_{\text{orb}}(\boldsymbol{k}_B) = 2\pi eB(n + 1/2 + \phi_B), \tag{8}$$

where $A_{\text{orb}}(\boldsymbol{k}_B)$ is the area of the cyclotron orbit with $\boldsymbol{k}_B$ the wave vector along the $\boldsymbol{B}$ direction, and ϕ_B is the Berry phase accumulated by the electrons during the cyclotron motion [77,78]. From the previous analysis, the knot Wilson loop integral precisely corresponds to the sum of the Berry phases ϕ_B accumulated by each cyclotron orbit. Therefore, we see that the Berry phase ϕ_B is π in this case. Under the renormalization of disorder, the linked nodal loops are separated, resulting in $\phi_B = 0$. The difference in the Berry phase ϕ_B thus induces the π Berry phase shift in the de Haas-van Alphen oscillation experiment as depicted in the right panel of Fig. 5. Therefore, these accumulated Berry phases ϕ_B for each nodal loop are unique for knotted nodal lines. If all the information of ϕ_B can be obtained, the nodal-knot structure can be determined to a large extent.

6. Discussions

Nodal line semimetals with non-trivial knotted or linked structures have been confirmed to exist in solid materials, such as Co_2-

Table 1
Summary of the emergent knot transitions for various (p,q) triggered by different types of disorders.

Disorder type	(p,q)			
	$(2,2)$	$(2,3)$	$(3,2)$	$(3,3)$
Clean	Hopf link	Trefoil knot	Trefoil knot	Valknut
Δ_0	Unknot	Unknot	Unknot	Unknot
Δ_x	Unknot	Hopf link	Unknot	Trefoil knot
Δ_y	2-Unlink	Unknot	3-Unlink	Unknot
Δ_z	2-Unlink	Hopf link	3-Unlink	Trefoil knot

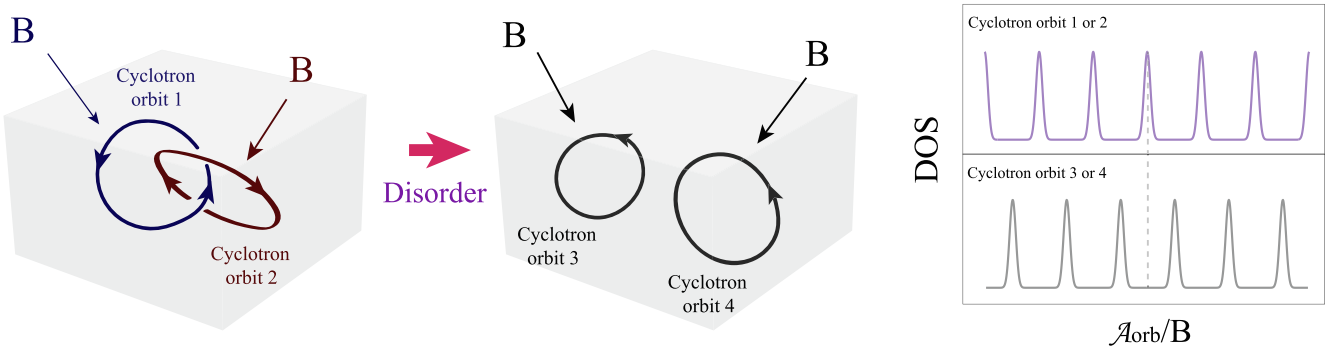

Fig. 5. Schematic diagram of utilizing the de Haas-van Alphen oscillation experiment to reflect the nodal-knot transitions. Before the transition, a magnetic field is applied perpendicular to one of the nodal loops (which is also the 1D Fermi surface). Electrons undergo cyclotron motion in momentum space, moving perpendicular to the magnetic field and around the nodal loop (left). The area enclosed by its cyclotron orbit in momentum space is denoted by A_{orb}. Sweeping B leads to the oscillations of DOS with period A_{orb}/B (right). Under the renormalization of disorder, the linked structure evolves to be unlinked (middle). The phase of the oscillation with A_{orb}/B shifted by a π Berry phase.

MnGa through ARPES experiments [11,29]. In the presence of disorder, the ARPES observations would be affected by the renormalization of the low-energy band structure. Our work predicts the possibility of disorder induced nodal-knot transitions under doping with magnetic or non-magnetic disorders, which awaits further experimental verification.

Aside from the solid materials, it is also achievable to introduce and control disorders in artificial systems such as cold atoms or acoustic and optical systems [32,40,46]. Especially, introducing noise in cold atoms, or utilizing the optical speckle field can simulate the disorder effect [79]. Moreover, the optical Raman lattice can simulate the spin–orbital coupling, which can achieve the magnetic disorder potentials [35]. In these ways, the magnetization directions of the disorders can be controlled more easily. Therefore, our work provides theoretical support for future studies of knotted topological phases and disorder-induced knot transitions in these systems.

Conflict of interest

The authors declare that they have no conflict of interest.

Acknowledgments

This work was supported by the National Key R&D Program of China (2022YFA1403700), the Innovation Program for Quantum Science and Technology (2021ZD0302400), the National Natural Science Foundation of China (12350402, 12304074, 12234017, and 12525401), the Guangdong Province (2020KCXTD001), the Guangdong Basic and Applied Basic Research Foundation (2023B0303000011), the Guangdong Provincial Quantum Science Strategic Initiative (GDZX2201001 and GDZX2401001), the Science, Technology and Innovation Commission of Shenzhen Municipality (ZDSYS20190902092905285), and the New Cornerstone Science Foundation through the XPLORER PRIZE, and Center for Computational Science and Engineering of SUSTech. Ming Gong was also supported by the China National Postdoctoral Program for Innovative Talents (BX20240004). We acknowledge helpful discussions with Robert-Jan Slager, Qing-Feng Sun, Hua Jiang, Chui-Zhen Chen, Zhenyu Xiao, and Xinchi Zhou.

Author contributions

Ming Gong and Peng-Lu Zhao conceived the idea from discussions with Hai-Zhou Lu. Ming Gong performed calculations with assistance from Peng-Lu Zhao. Ming Gong and Peng-Lu Zhao wrote the manuscript with contributions from all authors. Hai-Zhou Lu, Qian Niu, and X. C. Xie supervised the project.

Appendix A. Supplementary material

Supplementary data to this article can be found online at https://doi.org/10.1016/j.scib.2025.04.061.

References

[1] Baez JC, Muniain JP. Gauge fields, knots and gravity. Singapore: World Scientific; 1994.
[2] Simon SH. Topological quantum. Oxford: Oxford University Press; 2023.
[3] Atiyah MF. Topological quantum field theory. Publ Math Paris 1988;68:175–86.
[4] Witten E. Topological quantum field theory. Commun Math Phys 1988;117:353–86.
[5] Witten E. Quantum field theory and the Jones polynomial. Commun Math Phys 1989;121:351–99.
[6] Blanchet C, Habegger N, Masbaum G, et al. Topological quantum field theories derived from the Kauffman bracket. Topology 1995;34:883–927.
[7] Nayak C, Simon SH, Stern A, et al. Non-Abelian anyons and topological quantum computation. Rev Mod Phys 2008;80:1083–159.
[8] Eto M, Hamada Y, Nitta M, et al. Tying knots in particle physics; arXiv:2407.11731. 2024.
[9] Burkov AA, Hook MD, Balents L, et al. Topological nodal semimetals. Phys Rev B 2011;84:235126.
[10] Fang C, Weng HM, Dai X, et al. Topological nodal line semimetals. Chin Phys B 2016;25:117106.
[11] Chang GQ, Xu SY, Zhou XT, et al. Topological Hopf and chain link semimetal states and their application to Co_2MnGa. Phys Rev Lett 2017;119:156401.
[12] Bi R, Yan ZB, Lu L, et al. Nodal-knot semimetals. Phys Rev B 2017;96:201305(R).
[13] Ezawa M. Topological semimetals carrying arbitrary hopf numbers: Fermi surface topologies of a Hopf link, Solomon's knot, trefoil knot, and other linked nodal varieties. Phys Rev B 2017;96:041202(R).
[14] Yan ZB, Bi R, Shen HT, et al. Nodal-link semimetals. Phys Rev B 2017;96:041103(R).
[15] Lian B, Vafa C, Vafa F, et al. Chern-Simons theory and Wilson loops in the Brillouin zone. Phys Rev B 2017;95:094512.
[16] Ahn J, Kim D, Kim Y, et al. Band topology and linking structure of nodal line semimetals with Z_2 monopole charges. Phys Rev Lett 2018;121:106403.
[17] Wu QS, Soluyanov AA, Bzdušek T, et al. Non-Abelian band topology in noninteracting metals. Science 2019;365:1273–7.
[18] Yang ZS, Chiu CK, Fang C, et al. Jones polynomial and knot transitions in Hermitian and non-Hermitian topological semimetals. Phys Rev Lett 2020;124:186402.
[19] Bouhon A, Bzdušek T, Slager RJ, et al. Geometric approach to fragile topology beyond symmetry indicators. Phys Rev B 2020;102:115135.
[20] Bouhon A, Lange GF, Slager RJ, et al. Topological correspondence between magnetic space group representations and subdimensions. Phys Rev B 2021;103:245127.
[21] Bouhon A, Wu QS, Slager RJ, et al. Non-Abelian reciprocal braiding of Weyl points and its manifestation in ZrTe. Nat Phys 2020;16:1137–43.
[22] Peng B, Bouhon A, Monserrat B, et al. Phonons as a platform for non-Abelian braiding and its manifestation in layered silicates. Nat Commun 2022;13:423.
[23] Jankowski WJ, Noormandipour M, Bouhon A, et al. Disorder-induced topological quantum phase transitions in multigap Euler semimetals. Phys Rev B 2024;110:064202.
[24] Chowdhury D. Phase transition from Weyl to knotted semimetal using bicircular laser; arXiv:2411.12496. 2024.
[25] Kim S, Choi Y, Lim H, et al. Unconventional topological phase transition of the Hopf insulator; arXiv:2410.04021. 2024.

[26] Bzdušek T, Wu QS, Rüegg A, et al. Nodal-chain metals. Nature 2016;538:75–8.
[27] Sun XQ, Lian B, Zhang SC, et al. Double helix nodal line superconductor. Phys Rev Lett 2017;119:147001.
[28] Li CQ, Wang CM, Wan B, et al. Rules for phase shifts of quantum oscillations in topological nodal-line semimetals. Phys Rev Lett 2018;120:146602.
[29] Belopolski I, Chang GQ, Cochran TA, et al. Observation of a linked-loop quantum state in a topological magnet. Nature 2022;604:647–52.
[30] Ding YR, Xu DH, Chen CZ. Disorder-induced phase transitions in higher-order nodal line semimetals; arXiv:2401.13443v1. 2024.
[31] Wang C, Zhang PF, Chen X, et al. Scheme to measure the topological number of a Chern insulator from quench dynamics. Phys Rev Lett 2017;118:185701.
[32] Deng DL, Wang ST, Sun K, et al. Probe knots and Hopf insulators with ultracold atoms. Chin Phys Lett 2018;35:013701.
[33] Tarnowski M, Ünal FN, Fläschner N, et al. Measuring topology from dynamics by obtaining the Chern number from a linking number. Nat Commun 2019;10:1728.
[34] Ünal FN, Eckardt A, Slager RJ, et al. Hopf characterization of two-dimensional Floquet topological insulators. Phys Rev Res 2019;1:022003(R).
[35] Song B, He CC, Niu S, et al. Observation of nodal-line semimetal with ultracold fermions in an optical lattice. Nat Phys 2019;15:911–6.
[36] Ünal FN, Bouhon A, Slager RJ, et al. Topological Euler class as a dynamical observable in optical lattices. Phys Rev Lett 2020;125:053601.
[37] Leach J, Dennis MR, Courtial J, et al. Knotted threads of darkness. Nature 2004;432:165.
[38] Irvine WTM, Bouwmeester D. Linked and knotted beams of light. Nat Phys 2008;4:716–20.
[39] Kedia H, Bialynicki-Birula I, Peralta-Salas D, et al. Tying knots in light fields. Phys Rev Lett 2013;111:150404.
[40] Yang EC, Yang B, You OB, et al. Observation of non-Abelian nodal links in photonics. Phys Rev Lett 2020;125:033901.
[41] Jayaseelan M, Murphree JD, Schultz JT, et al. Topological atom optics and beyond with knotted quantum wavefunctions. Commun Phys 2024;7:1–9.
[42] Bode B. Complex optical vortex knots; arXiv:2407.19443. 2024.
[43] Yan QH, Liu RJ, Yan ZB, et al. Experimental discovery of nodal chains. Nat Phys 2018;14:461–4.
[44] Jiang B, Bouhon A, Lin ZK, et al. Experimental observation of non-Abelian topological acoustic semimetals and their phase transitions. Nat Phys 2021;17:1239–46.
[45] Qiu HH, Zhang QC, Liu TZ, et al. Minimal non-Abelian nodal braiding in ideal metamaterials. Nat Commun 2023;14:1261.
[46] Zhang QC, Li YT, Sun HF, et al. Observation of acoustic non-Hermitian Bloch braids and associated topological phase transitions. Phys Rev Lett 2023;130:017201.
[47] Jiang B, Bouhon A, Wu SQ, et al. Observation of an acoustic topological Euler insulator with meronic waves. Sci Bull 2024;69:1653–9.
[48] Lee CH, Sutrisno A, Hofmann T, et al. Imaging nodal knots in momentum space through topolectrical circuits. Nat Commun 2020;11:4385.
[49] Zhang X, Li GJ, Liu YH, et al. Tidal surface states as fingerprints of non-Hermitian nodal knot metals. Commun Phys 2021;4:1–10.
[50] Wang Z, Zeng XT, Biao YC, et al. Realization of a Hopf insulator in circuit systems. Phys Rev Lett 2023;130:057201.
[51] Carlström J, Stålhammar M, Budich JC, et al. Knotted non-Hermitian metals. Phys Rev B 2019;99:161115(R).
[52] Yang ZS, Hu JP. Non-Hermitian Hopf link exceptional line semimetals. Phys Rev B 2019;99:081102(R).
[53] Hu HP, Zhao EH. Knots and non-Hermitian Bloch bands. Phys Rev Lett 2021;126:010401.
[54] Bergholtz EJ, Budich JC, Kunst FK, et al. Exceptional topology of non-Hermitian systems. Rev Mod Phys 2021;93:015005.
[55] Patil YSS, Höller J, Henry PA, et al. Measuring the knot of non-Hermitian degeneracies and non-commuting braids. Nature 2022;607:271–5.
[56] Guo CX, Chen S, Ding K, et al. Exceptional non-Abelian topology in multiband non-Hermitian systems. Phys Rev Lett 2023;130:157201.
[57] Chen JZ, Wang Z, Tan YT, et al. Machine learning of knot topology in non-Hermitian band braids. arxiv.2401.10908. 2024.
[58] Zhu BF, Wang Q, Wang Y, et al. Versatile braiding of non-Hermitian topological edge states; arXiv:2406.00726. 2024.
[59] Kane CL, Mele EJ. Quantum spin Hall effect in graphene. Phys Rev Lett 2005;95:226801.
[60] Fu L, Kane CL, Mele EJ, et al. Topological insulators in three dimensions. Phys Rev Lett 2007;98:106803.
[61] Fu L, Kane CL. Topological insulators with inversion symmetry. Phys Rev B 2007;76:045302.
[62] Lee PA, Ramakrishnan TV. Disordered electronic systems. Rev Mod Phys 1985;57:287–337.
[63] Altland A, Simons BD. Condensed matter field theory. 2nd ed. Cambridge: Cambridge University Press; 2010.
[64] Volovik GE. The universe in a helium droplet. Oxford: Clarendon Press; 2003.
[65] Ludwig AWW, Fisher MPA, Shankar R, et al. Integer quantum Hall transition: an alternative approach and exact results. Phys Rev B 1994;50:7526–52.
[66] Wegner F. The mobility edge problem: continuous symmetry and a conjecture. Z Phys B: Condens Matter 1979;35:207–10.
[67] Cardy J. Scaling and renormalization in statistical physics. Cambridge: Cambridge University Press; 1996.
[68] Kardar M. Statistical physics of fields. Cambridge: Cambridge University Press; 2007.
[69] Thouless DJ, Kohmoto M, Nightingale MP, et al. Quantized Hall conductance in a two-dimensional periodic potential. Phys Rev Lett 1982;49:405–8.
[70] Slager RJ, Juričič V, Roy B, et al. Dissolution of topological Fermi arcs in a dirty Weyl semimetal. Phys Rev B 2017;96:201401.
[71] Pixley JH, Huse DA, Das Sarma S, et al. Rare-region-induced avoided quantum criticality in disordered three-dimensional Dirac and Weyl semimetals. Phys Rev X 2016;6:021042.
[72] Roy B, Slager RJ, Juričič V, et al. Global phase diagram of a dirty Weyl liquid and emergent superuniversality. Phys Rev X 2018;8:031076.
[73] Hu J, Tang ZJ, Liu JY, et al. Evidence of topological nodal-line fermions in ZrSiSe and ZrSiTe. Phys Rev Lett 2016;117:016602.
[74] Ali MN, Schoop LM, Garg C, et al. Butterfly magnetoresistance, quasi-2D Dirac Fermi surface and topological phase transition in ZrSiS. Sci Adv 2016;2:e1601742.
[75] Pezzini S, van Delft MR, Schoop LM, et al. Unconventional mass enhancement around the Dirac nodal loop in ZrSiS. Nat Phys 2018;14:178–83.
[76] Shi L, Liu XX, Wang CM, et al. Quantum oscillation in Hopf-link semimetals; arXiv:2412.07122. 2024.
[77] Xiao D, Chang MC, Niu Q, et al. Berry phase effects on electronic properties. Rev Mod Phys 2010;82:1959–2007.
[78] Mikitik GP, Sharlai YV. Manifestation of Berry's phase in metal physics. Phys Rev Lett 1999;82:2147–50.
[79] Kondov SS, McGehee WR, Zirbel JJ, et al. Three-dimensional Anderson localization of ultracold matter. Science 2011;334:66–8.